Optical absorbance and band-gap engineering of $(BN)_{1-x}(C_2)_x$ two-dimensional alloys: Phase separation and composition fluctuation effects

I. Guilhon,* M. Marques,† and L. K. Teles‡
Grupo de Materiais Semicondutores e Nanotecnologia, Instituto Tecnológico de Aeronáutica, DCTA, 12228-900 São José dos Campos, Brazil

F. Bechstedt
Institut für Festkörpertheorie und -optik, Friedrich-Schiller-Universität, Max-Wien-Platz 1, D-07743 Jena, Germany
(Received 1 August 2016; revised manuscript received 3 November 2016; published 10 January 2017)

The $(BN)_{1-x}(C_2)_x$ alloys are promising materials for band-gap engineering in two-dimensional electronics. In this work, we provide a complete scenario of statistical possibilities for the distribution of atoms and its influence on electronic and optical properties. Using first-principles calculations combined with the generalized quasichemical approximation to account for disorder effects, we study the properties of these two-dimensional alloys as a function of their average composition. Our results show that atomic arrangements with C-C and B-N bonds are energetically favored over the ones with B-B and N-N bonds, explaining the known tendency to phase separation, verified by a T-x phase diagram. We calculate the energy gap as a function of the composition considering both composition fluctuation and phase separation effects. Experimental data are discussed in this context. Finally, we obtain absorption spectra reproducing a two-peak pattern for intermediate carbon concentrations found experimentally and identified with phase-segregated instead of homogeneous alloys.

DOI: 10.1103/PhysRevB.95.035407

I. INTRODUCTION

The need for materials with customized electronic band structure asks for powerful tools for reliable predictions. Novel devices can be conceived and designed for superior performance. One of the widely applied approaches for band engineering is alloying of two or more semiconductors, which has been used in numerous optoelectronic applications. The alloy properties can be tuned between those observed in the end components by controlling the average composition as well as composition fluctuations.

With increasing research interest in two-dimensional (2D) materials, 2D alloys have received considerable attention and have been synthesized [1–7]. Among several possibilities, hexagonal boron nitride (h-BN) is a natural candidate to be combined with graphene in a 2D alloy, since both sheet crystals possess a flat honeycomb structure while the lattice constant mismatch only amounts to 2% [8]. In contrast to graphene, which has no energy gap, h-BN is a dielectric with a wide energy band gap of about 6 eV [9] due to the strongly ionic B-N bond and the broken symmetry of the two sublattices in h-BN. Alloying these two 2D materials allows, in principle, a very wide range for changing the energy gap.

Recently, it has been demonstrated that $(BN)_{1-x}(C_2)_x$ layers can be synthesized by chemical vapor deposition (CVD) [5,6] or via chemical substitution of C with h-BN in graphene [7]. However, the distributions of atoms in these alloys are far away from perfectly random, instead interpreted in terms of phase separation resulting in h-BN-rich and graphene-rich domains [5,6,10].

The alloy thermodynamics determines the miscibility of the combined materials, thereby also favoring some specific atomic arrangements, which might have a strong influence on the electronic and optical properties of the alloy with a given composition x. Depending on the size of the domains produced in the phase segregation process, their effect on the observed properties of $(BN)_{1-x}(C_2)_x$ might be different. According to Ci *et al.* [5], for domain sizes smaller than 2–3 nm, the film behaves like a BN-C alloy, with a band gap equal to the average gap of the two components, while domain sizes larger than 2–3 nm can lead to carrier localization and exhibit the electronic and optical properties of both materials.

Despite the importance of such microstructural features for electronic properties, the actual theoretical studies of $(BN)_{1-x}(C_2)_x$ monolayer alloys have been restricted to investigate "guessed" nonrandom structures [11–14]. Statistical approaches have been used only to predict phase separation [10,14,15], but its effects on electronic and optical properties is still an open question. Therefore, the combination of a quasiparticle electronic structure method with a statistical approach that takes into account the segregation and composition fluctuations should give rise to novel results for the prediction of the fundamental energy gap and related electronic as well as optical properties.

In this paper, we perform a rigorous and systematic theoretical study of $(BN)_{1-x}(C_2)_x$ monolayer alloys, considering different local atomic configurations and their statistical probabilities to account for disorder effects. Their phase stability is studied through the temperature versus composition phase diagram. For different compositions the electronic and optical properties are predicted and discussed in the light of the phase-separated alloys.

II. METHODOLOGY

To account for composition and disorder effects, we consider the generalized quasichemical approximation (GQCA), which has been successfully applied to different 2D and

*ivanguilhonn@gmail.com
†mmarques@ita.br
‡lkteles@ita.br

3D alloys [16–18]. In the framework of this method, an alloy is described by an average of a set of statistically independent clusters. All the possible cluster configurations with $2n = 8$ atoms are organized in J different nonequivalent classes with different numbers of degeneracy g_j. Two cluster atomic arrangements are said to be equivalent if they have the same physical properties. The equivalence of their atomic arrangement is identified by the application of all symmetry operations.

The probabilities of occurrence $x_j(x,T)$ of each cluster class j at an average composition x and growth temperature T are determined by the minimization of the mixing free energy of the alloy as described elsewhere [16,17,19,20]. The $(BN)_{1-x}(C_2)_x$ system is modeled as a ternary alloy with $x_C = x$ and $x_B = x_N = (1-x)/2$.

The mixing free energy of an alloy per cluster can be written as $\Delta F = \Delta U - T\Delta S$, where ΔU is the mixing internal energy and the ΔS is the configurational entropy. Each cluster class is characterized by its total energy ε_j ($j = 0,1,2,3,\ldots,J$). The excess energy $\Delta\varepsilon_j$ for the formation of the cluster j, with $2n_j$ C atoms and $(n-n_j)$ B as well as N ones, can be defined as

$$\Delta\varepsilon_j = \varepsilon_j - \frac{n_j}{n}\varepsilon_C - \left(1 - \frac{n_j}{n}\right)\varepsilon_{h-BN}, \tag{1}$$

where ε_C and ε_{h-BN} are the total energy of graphene and h-BN clusters, respectively. For low temperatures the alloy mixing free energy is dominated by ΔU and the probability distribution x_j is concentrated on the configurations j with lower excess energies ε_j and the constituent components do not alloy. As the temperature grows, the entropy term $-T\Delta S$ becomes more important. The mixing entropy is given as

$$\begin{aligned}\Delta S(x,T) = &-2nk_B[x_C \ln x_C + x_B \ln x_B + x_N \ln x_N] \\ &- k_B D_{KL}\left(x_j | x_j^0\right),\end{aligned} \tag{2}$$

where

$$D_{KL}\left(x_j || x_j^0\right) = \sum_{j=0}^{J} x_j \log\left(\frac{x_j}{x_j^0}\right) \tag{3}$$

is the relative entropy, or the Kullback-Leibler (KL) divergence [21], between the random cluster probability distribution $x_j^0(x)$ in the ideal solution and the probability distribution $x_j(x,T)$ obtained from the excess free energy minimization.

In general, a property $p(x,T)$ of a certain alloy can be calculated as an average of the property values p_j weighted by occurrence probabilities $x_j(x,T)$ as

$$p(x,T) = \sum_{j=0}^{J} x_j(x,T)p_j. \tag{4}$$

Thereby, the set of probabilities $x_j(x,T)$ must fulfill two constraints, (i) the normalization of the sum of all probabilities and (ii) the average composition x, which follows if p_j is replaced by n_j. The constrained minimization of the excess free energy rules the probability for realization of a cluster configuration j,

$$x_j(x,T) = \frac{g_j \lambda^{n_j} \exp(-\beta\Delta\varepsilon_j)}{\sum_{j=0}^{J} g_j \lambda^{n_j} \exp(-\beta\Delta\varepsilon_j)}, \tag{5}$$

where $\beta = 1/kT$ and λ is a numerical parameter determined by the average composition constraint $\sum_{j=0}^{J} n_j x_j = nx$.

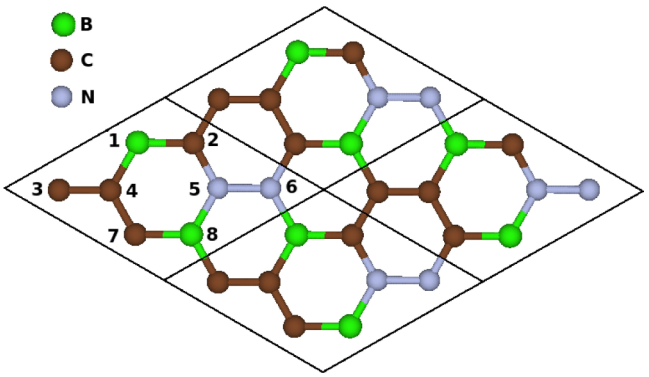

FIG. 1. Illustration of a 2D periodic system for a given atomic configuration with $n_j = 2$. B, C, and N atoms are represented as green, brown, and gray dots, respectively. Four supercells are displayed. The atomic sites are labeled by 1,2,3,4,5,6,7,8. Consequently, the represented configuration is BCCCNNCB.

In this work, the clusters $B_{n-n_j}N_{n-n_j}C_{2n_j}$ ($n_j = 0,1,2,3,4$) are defined as flat hexagonal 2×2 unit cells as depicted in Fig. 1, where the labeling of the cluster atoms is also explained. The atomic sites can be randomly occupied by boron, carbon, or nitrogen atoms. The clusters cover all the configurations with equal numbers of boron and nitrogen atoms. Besides C-C, B-N, C-B, and C-N bonds, also B-B and N-N ones are allowed. They result in 1107 possible atomic configurations, which can be arranged into 43 classes with different degeneracies applying all the space group symmetry operations. Such systems with equal numbers of boron and nitrogen atoms are synthesized by means of CVD growth using ammonia borane NH_3-BH_3 as a single precursor of boron and nitrogen atoms [5] or controlling the flux of distinct boron and nitrogen precursors [22].

In order to analyze the thermodynamic stability of the alloy, the T-x phase diagram is constructed from the mixing free energy, as described elsewhere [16,17]. Each point in the diagram represents one alloy with a carbon composition x grown at a temperature T. The binodal and the spinodal curves split the plane in three regions, which correspond to stable, metastable, and unstable phases. In the region below the spinodal curve the alloy decomposes into two different phases with average compositions x_1 and x_2 thereby minimizing the mixing free energy $F(x,T)$ for given x and T. The poor and rich phases with concentrations x_1 and x_2 are respectively characterized by statistical weights

$$w_1 = \frac{x_2 - x}{x_2 - x_1} \quad \text{and} \quad w_2 = \frac{x - x_1}{x_2 - x_1}. \tag{6}$$

If the phase segregation process occurs and the obtained domain sizes are larger than the cluster dimensions, distinct occurrence probability distributions $x_j(x_1,T)$ and $x_j(x_2,T)$ can be associated with the poor and rich phases, respectively. If an

average property is defined for such a $(BN)_{1-x}(C_2)_x$ system, we estimate it as the weighted average of the two decomposed phases according to their weights w_1 and w_2.

Between the binodal and spinodal curves the alloy is metastable and the phase decomposition is hampered. The critical temperature T_c is defined as the smallest temperature for which the alloy is still thermodynamically stable at any composition.

The total energy ε_j of each cluster class j is calculated within the *ab initio* density functional theory (DFT), as implemented in the VASP code [23,24]. In each cluster calculation we consider a periodic system whose unit cells are represented by one cluster class. A 2D supercell with a possible atomic arrangement is displayed in Fig. 1 for a stoichiometric ratio of $n_j = 2$. Each alloy system is simulated as an artificial 3D crystal constituted by a periodic repetition of the atomic sheets in a distance $L = 20$ Å from the neighbor ones. This distance is large enough that the interaction between the sheets vanishes.

The generalized gradient approximation (GGA) as proposed by Perdew-Burke-Ernzerhof (GGA-PBE) [25,26] is applied to calculate the exchange and correlation (XC) energy. Pseudopotentials for the B, C, and N cores and all-electron wave functions are generated within the projector-augmented wave (PAW) method [27,28]. The wave functions between the cores are expanded in plane waves with a kinetic energy cutoff of 450 eV. Integrals over the Brillouin zone (BZ) are calculated considering a $12 \times 12 \times 1$ Γ-centered Monkhorst-Pack k-point mesh [29]. In order to find the equilibrium configuration lateral lattice constants, all atomic coordinates are relaxed until the Hellmann-Feynman forces are smaller than 0.01 eV $Å^{-1}$.

It is well known that the pure DFT methodology tends to underestimate the energy gaps, mainly due to the neglect of the nonlocality of the XC potential. Therefore a trustworthy prediction for electronic and optical properties demands corrections on standard DFT calculations to take the excitation aspect into account [30]. In this study we perform a simulation of the quasiparticle corrections for the different atomic configuration considering a hybrid functional proposed by Heyd, Scuseria, and Ernzerhof (HSE06) [31,32].

The optical properties are described by the frequency-dependent dielectric matrix, which is calculated within the independent-quasiparticle approximation [33]. The optical transition matrix elements are described adopting the longitudinal gauge [34]. We focus on the optical absorbance $A(\omega)$ for normal incident light with frequency ω. It is connected to the frequency-dependent imaginary part of the in-plane component of the dielectric function $\epsilon_j(\omega)$ of the artificial 3D crystal used to simulate the cluster class j. Interestingly, the 2D quantity $A_j(\omega)$ becomes independent of the layer distance L in the artificial 3D crystal,

$$A_j(\omega) = \frac{\omega}{c} L \,\mathrm{Im}[\epsilon_j(\omega)], \tag{7}$$

where c is the speed of light in vacuum. More generally, this quantity is the real part of 2D optical conductivity. However, in the limit of vanishing reflectance it is identical with the absorbance [35].

Spectra of various mixtures of graphene and h-BN were predicted in the paper of Bhowmick *et al.* [36], but their results do not consider effects due to the alloy thermodynamics, being restricted to simple averages between the K-edge x-ray absorption spectra observed for arbitrary atomic arrangements of the alloys and the pure end components. In the GQCA formalism, an absorbance spectrum $A_j(\omega)$ is calculated in the *ab initio* framework for each chosen cluster configuration j. The average absorbance spectra of an alloy are estimated within GQCA by Eq. (4). Because of the strong segregation tendencies in $(BN)_{1-x}(C_2)_x$, in particular, we study the optical properties of a subset S of all cluster configurations of a $(BN)_{1-x}(C_2)_x$ alloy where B-B and N-N do not occur. Since the normalization $\sum_{j\in S} x_j = 1$ used in Eq. (4) is not necessarily valid, we define a renormalized quantity

$$A_{GQCA}(\omega,x,T) = \frac{\sum_{j\in S} x_j(x,T) A_j(\omega)}{\sum_{j\in S} x_j(x,T)}. \tag{8}$$

This definition should be reasonable to represent homogeneous systems under stable (x,T) conditions and systems with small cluster sizes where composition fluctuation effects between the two segregated phases are relevant. If these conditions are not fulfilled and the system is fully segregated in poor and rich phases, i.e., for temperatures and compositions below the binodal curve, a more reliable estimation of the mean absorbance spectra is given by

$$\begin{aligned} A_{PS}(\omega,x,T) = {} & w_1(x,T) A_{GQCA}(\omega,x_1,T) \\ & + w_2(x,T) A_{GQCA}(\omega,x_2,T) \end{aligned} \tag{9}$$

with w_1 and w_2 the statistical weights defined in Eqs. (6).

III. RESULTS AND DISCUSSION

A. Phase stability and composition fluctuation

In a macroscopic alloy the mixing free energy $\Delta F(x,T)$ is determined by the interplay between configurational entropy and internal energy resulting in the temperature- and composition-dependent cluster probabilities $x_j(x,T)$. Thereby, the most favorable local arrangement of atoms is influenced by the alloy thermodynamics, favoring some cluster configurations with low excess energies in preference of others. The plot of the excess energies $\Delta\varepsilon_j$ of the 43 considered cluster configurations as a function of the carbon concentration is depicted in Fig. 2. We verify that the configurations with B-B and N-N bonds, represented as black diamonds in Fig. 2, are strongly energetically unfavorable. The most energetically favorable configurations are the atomic arrangements BNBNBNBN ($n_j = 0$), CCBNBNBNBN ($n_j = 1$), CCCCBNBN ($n_j = 2$), CCCCCCBN ($n_j = 3$), and CCCCCCCC ($n_j = 4$). They show a significant tendency to maximize the number of C-C and B-N bonds, in detriment of C-N and C-B ones, in agreement with reports in previous theoretical [10] and experimental [37] works. Consequently, the cluster configurations which represent almost a mixture of h-BN and graphene are energetically favored. This fact explains the very strong tendency of the mixed system to segregate into graphene

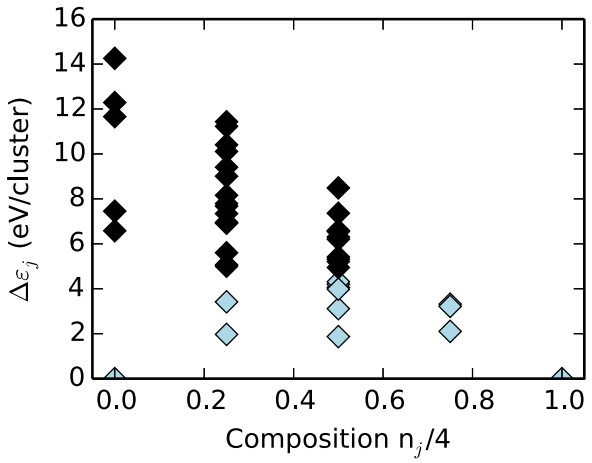

FIG. 2. Excess energies $\Delta\varepsilon_j$ of each atomic configuration as function of the number of carbon atoms n_j. The black diamonds represent the configurations with mainly B-B and N-N bonds, while the light blue diamonds represent the complementary subset of the possible configurations.

and h-BN domains as observed experimentally [5], in spite of the very small lattice mismatch.

Figure 3 depicts the resulting phase diagram, in which we observe a huge critical temperature $T_c = 5200$ K, significantly above typical growth temperatures. This temperature is comparable to the result of $T_c = 4500$ K calculated using Monte Carlo simulations, neglecting the lattice vibrations, which is much higher than the expected melting point of the alloy [10]. The neglect of the vibrational contribution to the free energy of the alloy may result in an overestimation of the critical temperature and underestimation of the solubility [38]. Nevertheless, since the typical growth temperatures [22,39] are much lower than the calculated critical temperature T_c, a good agreement between our results and the experimental findings is observed.

The phase diagram in Fig. 3 shows that for not too high temperatures random alloys can only exist for extremely small

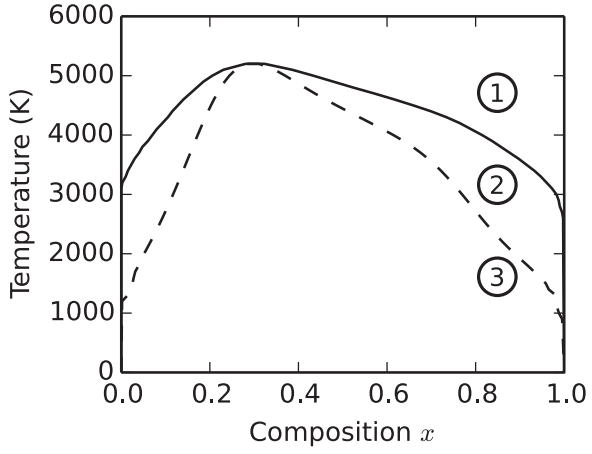

FIG. 3. The T-x phase diagram of $(BN)_{1-x}(C_2)_x$. The binodal (spinodal) curve is represented by the full (dashed) line. The stable, metastable, and unstable regions in the T-x diagram are labeled by 1, 2, and 3, respectively.

C or h-BN concentrations and that carbon-rich alloys are more thermodynamically favored than h-BN-rich ones. For a typical growth temperature of $T = 1600$ K, we predict a very small carbon solubility in h-BN of $x_C = 0.028$ and a h-BN solubility in graphene of $x_{BN} = 0.042$. These results are in very good agreement with the experimental values $x_C^{\text{exp}} = 0.032$ and $x_{BN}^{\text{exp}} = 0.05$ reported by Uddin *et al.* [22,39].

The probabilities $x_j(x,T)$ for the realization of a certain atomic configuration j depend mainly on the excess energies for lower temperatures. For higher temperatures the entropy term in the mixing free energy (2) becomes more important. The distribution of the occurrence probabilities among the 43 cluster classes starts to resemble the random distribution and more configurations can be statistically relevant depending on the considered growth temperature T. This behavior is depicted by bar histograms in Fig. 4 for an average composition $x = 0.5$ and increasing temperature T. In agreement with the excess energies, for lower temperatures the probability to find a cluster with B-B and N-N bonds is vanishingly small. For such temperatures, mainly the cluster classes with C-C, C-N, C-B, and B-N bonds in the subset S should be realized. Only for temperatures close to the critical one significant contributions from clusters with B-B and N-N bonds may also occur. In this case, the cluster distribution approaches the probabilities predicted for a random alloy, i.e., an ideal solid solution.

The similarity between the GQCA probability $x_j(x,T)$ and the probabilities of clusters j in an ideal solid solution $x_j^0(x)$ can be measured by the KL divergence $D_{KL}(x_j|x_j^0)$ given in Eq. (3).

This quantity rules the deviation of the actual mixing entropy from the one of the ideal system. Figure 5 shows the behavior of the KL divergence between the distributions at average compositions $x = 0.25$, 0.5, and 0.75 as a function of the temperature. The maximum divergence value at low temperatures corresponds to the occurrence of only graphene and ordered h-BN clusters. As the temperature increases the two materials start to alloy and the divergence decays. One observes in Fig. 5 that the alloy with carbon composition $x = 0.25$ requires the highest temperature to resemble the random alloy probability distribution, while the compositions $x = 0.50$ and $x = 0.75$ require smaller temperatures. This is consistent with the asymmetry observed in the calculated T-x phase diagram, as depicted in Fig. 3. The assumption of a random atomic distribution in a $(BN)_{1-x}(C_2)_x$ alloy is hardly justified for typical growth temperatures. This is in agreement with the phase diagram in Fig. 3 and the reported alloy tendency for phase segregation [5,6,10,22,39,40].

B. Structural parameters

We estimate the structural, electronic, and optical properties within the GQCA formalism considering a typical growth temperature of $T = 1600$ K as reported in the literature [5,22,39,40].

Initially the behavior of the alloy lattice parameter $a(x)$ as a function of the carbon concentration x was investigated. It was verified that $(BN)_{1-x}(C_2)_x$ alloys obey Vegard's law [41,42] at the considered growth temperature. The values $a(x,T)$ calculated within the GQCA approach only slightly deviate from the linear fit $a(x) = a_{BN}(1-x) + a_C x$, with

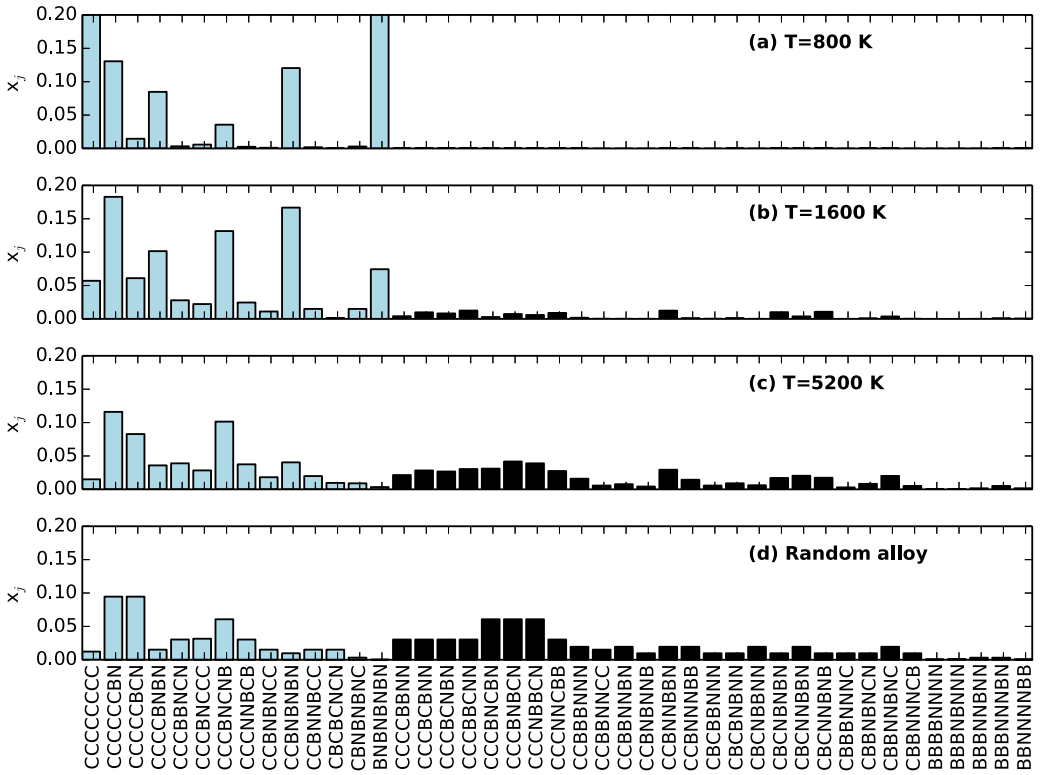

FIG. 4. The probability histogram of all cluster configuration classes of a $(BN)_{1-x}(C_2)_x$ alloy with $x = 0.5$ at 800 K (a), 1600 K (b), and 5200 K (c) within the GQCA formalism. A histogram obtained for a random alloy, more precisely an ideal solid solution, is depicted in (d). The black bars represent the configurations with B-B and N-N bonds, while the light blue bars represent the complementary configuration subset S.

$a_C = 2.47$ Å and $a_{BN} = 2.51$ Å, with a root-mean-squared error (RMSE) lower than 4×10^{-3} Å. The second structural property observed for the clusters is their buckling amplitude, which is defined as the maximum displacement of atoms from a flat configuration. The mean value of the buckling amplitude within GQCA is not larger than 3×10^{-3} Å, showing that the alloys preserve the planar hexagonal structure exhibited by its end components.

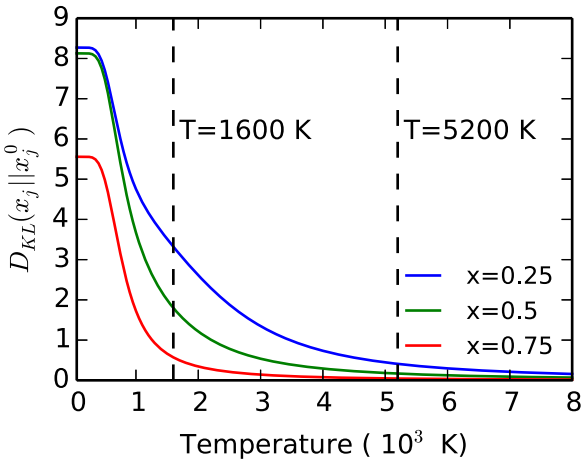

FIG. 5. Kullback-Leibler divergence between the ideal solid solution and GQCA probability distributions as a function of temperature for different compositions $x = 0.25$, 0.5, and 0.75. Small divergence values indicate similar probability distributions. The adopted growth temperature for alloy property estimations and the critical temperature are highlighted.

C. Electronic and optical properties

In Fig. 7 we plot the calculated fundamental energy gap curve together with the results $E_{g,j}$ for each cluster configuration. The values for the energy gaps of the CCBNBNNB, CBCNBBNN, CBBBNNNC, and BBBBNNNN configurations, which exhibit a metallic behavior, are considered to be zero, in agreement with the interpretation that graphene is a zero-gap semiconductor. Metallic behavior of clusters with B-B and N-N bonds is in agreement with reported results to some $B_xC_yN_z$ layered structures available in the literature [14]. However, considering the alloy statistics, these clusters do not have a dominant influence on the alloy properties.

Because of the high computational costs we restrict the electronic structure calculations using the hybrid functional HSE06 to the nine most statistically relevant configurations with the lowest excess energies in Fig. 2. The considered configuration classes are depicted in Fig. 6. They correspond to up to 99.6% of the total probability in the carbon-poor phase ($x_1' = 0.02$) and to 95.7% in the carbon-rich phase ($x_2' = 0.95$) at the considered growth temperature, according to GQCA calculations.

As expected, the HSE06 approach results in larger fundamental energy gaps in comparison with DFT-PBE calculations, as can be observed comparing the dotted black and the full blue energy gap curves in Fig. 7. Due the fact that only one configuration has a significant statistical weight at $x = 0$ and

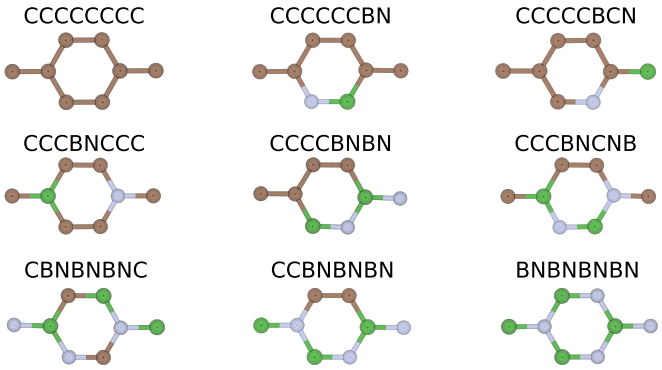

FIG. 6. Nine most statistically relevant cluster classes with low excess energies used for electronic structure and optical calculations using the HSE06 functional. The cluster labels are defined according to atomic site numeration defined in Fig. 1.

$x = 1$, the energy band gap curve varies between $E_{g,BN} = 6.06$ eV (4.64 eV) and $E_{g,C} = 0$ eV (0 eV) within the HSE06 (DFT-PBE) approach, corresponding to pure hexagonal boron nitride and pure graphene, respectively.

If the growth conditions are controlled so that domain sizes are comparable with the considered clusters, the GQCA calculations introduce the effect of local composition fluctuations and the solution of the Lagrange problem yields a set of probabilities $x_j(x,T)$ that gives the energy band gap curve represented by the blue solid line in Fig. 7, including only the composition fluctuation effect. We define a concentration-dependent bowing parameter $b(x)$ as a measure of the deviation

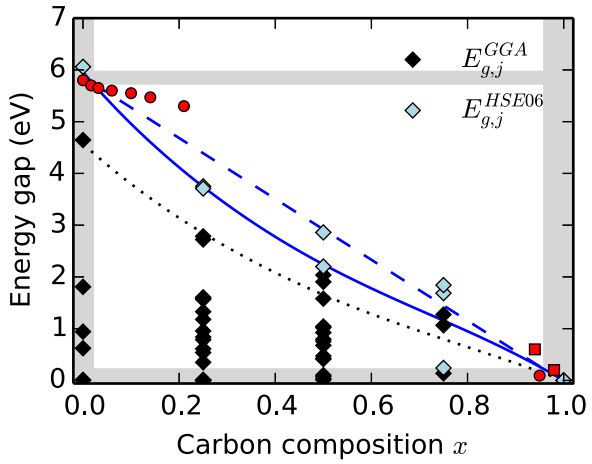

FIG. 7. The energy band gap as a function of the composition for $(BN)_{1-x}(C_2)_x$ alloys obtained with the GGA functional (dotted black curve) and within the HSE06 approach with and without phase decomposition effects (dashed and full blue lines, respectively). We emphasize that the dashed line can only be obtained for very small cluster domains, while larger cluster domain size would result in an emission near or within the shaded gray regions. The vertical gray shades indicate the x compositions where the alloy is stable and the horizontal ones correspond to the energy gap tune range at the stable composition conditions. The black and light blue diamonds represent the energy band gap obtained by GGA and HSE06 calculations for the investigated clusters. Available experimental data are represented by red circles [22,39] and squares [6].

from the linear behavior for the energy gap curve by fitting our results with the function $E_g(x,T) = (1-x)E_{g,BN} + xE_{g,C} - b(x)x(1-x)$. The calculated bowing parameter is $b(x) = (5.6 - 4.9x)$ eV, with a rms deviation of 0.02 eV. This finding is a generalization of the bowing parameters of 3.6 eV and 4.8 eV [22,39], estimated from the available experimental data for the fundamental energy gap of the two end components and samples of 1-μm-thick BC_2N ($x = 0.5$) films [43].

If the phase segregation results in domain sizes greater than the cluster sizes, one single set of probabilities $x_j(x,T)$ does not represent the decomposed alloy in BN-rich and carbon-rich phases. Each of these two phases has its own probability distribution $x_j(x_1,T)$ and $x_j(x_2,T)$, respectively, where x_1 and x_2 are given by the T-x phase diagram in Fig. 3. If the assumption that the domain sizes are not large enough so that an alloyed system is still obtained, we can estimate $E_g(x,T)$ as a weighted mean of the energy gaps of $E_g(x_1,T)$ and $E_g(x_2,T)$ of the carbon-poor and carbon-rich phases with respective weights w_1 and w_2 [in Eq. (6)]. Since the weights w_1 and w_2 vary linearly with the average composition x, $E_g(x,T)$ should vary linearly in the range $x_1 < x < x_2$ when phase segregation effects are included. This fact is represented by the blue dashed line in Fig. 7. However, our predictions of the energy gap as a function of the composition for the different phase separation regimes can also be useful for their identification, especially considering the more recent experimental technique that shows the possibility of controlling the domain sizes [8]. Recently, experimental results have indicated that if domain sizes are not controlled, distinct electronic properties corresponding to graphene and h-BN phases can be verified in a phase-separated system with composition about $x = 44\%$ [44].

As one can observe in Fig. 7, different energy gap values are possible for different cluster configurations with the same carbon concentration. This indicates that the use of a statistical approach to account for disorder effects is mandatory due the fact that a change of the atomic arrangement of atoms can result in entirely different electronic properties. Therefore, the choice of particular cluster configurations with a defined composition might not properly represent the chemically disordered system with an average composition x and composition fluctuations derived within the GQCA formalism. For example, when disorder effects are neglected and arbitrary arrangements are taken as the representation of the $(BN)_{1-x}(C_2)_x$ alloy, some results may suggest a nonmonotonic behavior of the energy gap as a function of the composition [12], which is not verified by our statistical approach.

The experimental results derived from optical absorption measurements [39] are also displayed in Fig. 7 and require further discussion. In Fig. 7 the shaded vertical regions represent the range of composition of a stable alloy without phase separation, and the horizontal ones their corresponding energy gaps. We observe that for carbon concentrations below the carbon solubility range, i.e., which gets into the shaded region, the experimental data fall on the theoretical curve and indicate a reduction of the energy gap with the increasing C content. In the case of carbon-rich alloys, our theoretical energy gap curve lies between the experimental findings [6,22].

However, for carbon concentrations above its solubility in h-BN, where the phase separation occurs, the decrease of the energy gap is much weaker than the estimated GQCA curve

(the full blue line), and stays near from the shaded area. The results can be explained in the light of the phase separation process, which may change the light emission mechanism. The light emission from the samples possibly comes from a decomposed phase with large domain sizes, leading to carrier localization, which explains why the energy gaps are larger than the average predicted by the dashed curve. This reflects the fact that investigation of such effects of phase segregation on optical and electronic properties depends on the domain sizes and shapes [13,37,44].

Optical measurements show two absorption edges for $(BN)_{1-x}(C_2)_x$ alloys with different carbon concentrations which can be associated with a carbon-rich and an h-BN-rich phase [5,6]. The relative intensities of the peaks depend on the alloy composition between the two end components, while their positions do not change appreciably with x.

We compare the calculated optical absorbance spectra $A_{GQCA}(\omega,x,T)$ [Fig. 8(a)] assuming only local composition fluctuation effects and the absorbance spectra $A_{PS}(\omega,x,T)$ [Fig. 8(b)] considering the phase segregation in the system.

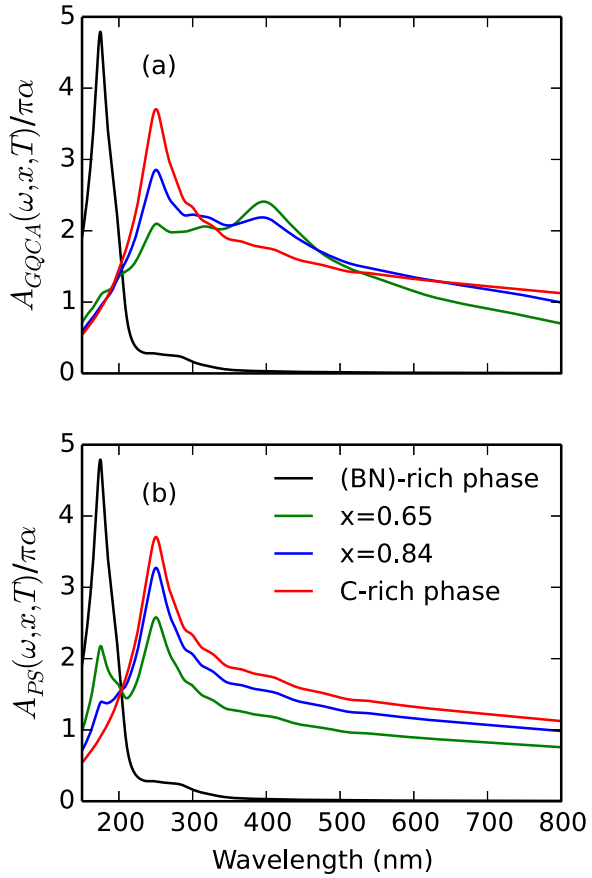

FIG. 8. Optical absorbance as a function of the wavelength for $(BN)_{1-x}(C_2)_x$ alloys with different carbon compositions. The red (black) full line stands for the carbon-rich (BN-rich) phase for comparison with intermediate compositions $x = 0.65$ and $x = 0.84$, represented by green and blue lines. The absorption spectra predictions are calculated considering local composition fluctuations (a) and complete phase segregation (b). The independent-quasiparticle approximation and HSE06 treatment are applied. The statistical weights are calculated considering a typical growth temperature of $T = 1600$ K.

The optical absorbance of the carbon-rich and BN-rich phases have distinct pronounced absorbance peaks in the considered wavelength region [5]. The peak of the carbon-rich phase at low wavelengths is associated with π-π^* transitions at the M points in the Brillouin zone of graphene [6,45], while the peak of the BN-rich phase is associated with the optical transitions between valence and conduction bands of h-BN in the UV region at the K and M points. In the long-wavelength limit the absorption almost vanishes for the h-BN-rich phase due to

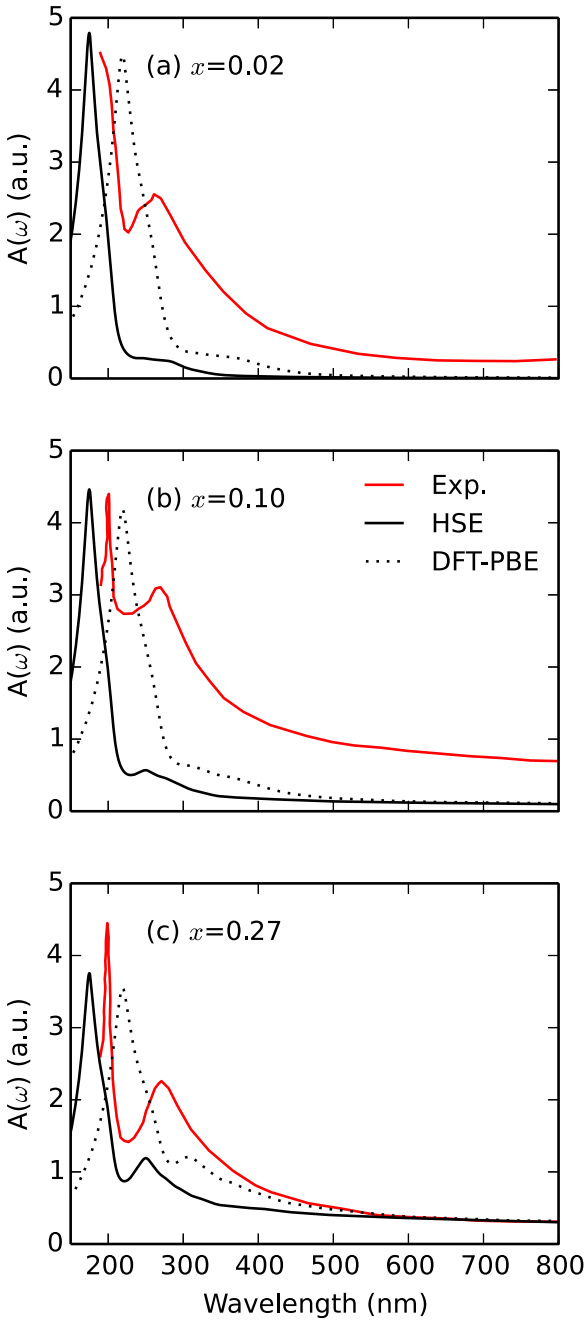

FIG. 9. Measured [6] (red solid line) and calculated (black solid line: HSE06, black dotted line: DFT-PBE) optical absorbance for $(BN)_{1-x}(C_2)_x$ with $x = 0.02$ (a), 0.10 (b), and 0.27 (c). The calculations have been performed within the independent-(quasi)particle approximation and assuming complete phase separation.

large gap, approaching 6 eV. On the contrary, in the case of the graphene-rich phase the in-plane absorbance reaches a value $\pi\alpha$ (α is the Sommerfeld fine structure constant). This has been demonstrated experimentally [46] and theoretically [47]. It goes back to the linear bands of graphene forming Dirac cones at the K and K′ points in the Brillouin zone [35,47].

The difference between the blue and green lines in Fig. 8(a) and Fig. 8(b) for average composition $x = 0.65$ and $x = 0.84$ shows a very strong effect of phase decomposition on the absorbance spectrum of alloys with intermediate compositions. When small clusters and composition fluctuations are assumed in Fig. 8(a), clusters with intermediary composition and lower fundamental energy gap are favored. Therefore, besides a reduction of the intensity of the graphene absorption peak additional redshifted absorption peaks appear, which however are not experimentally observed [5,6]. Otherwise, if the phase segregation is considered as in Fig. 8(b), the absorbance spectra $A_{PS}(\omega,x,T)$ are given by a weighted mean between the spectra of the two segregated phases and have the same qualitative behavior as the experimental findings [5,6].

Because of the tendency for compensation of quasiparticle and excitonic effects [48] the measured peaks appear between the HSE06 and DFT-PBE curves, as depicted in Fig. 9. Also the number of peaks (or shoulders) agrees in the experimental and theoretical spectra. Differences in intensities may be traced back to the fact that in calculations a substrate with refraction index 1, i.e., vacuum, has been assumed. The best qualitative agreement with respect to the line shape can be verified for the sample with $x = 0.27$.

Our results confirm the strong evidence for the $(BN)_{1-x}(C_2)_x$ phase segregation in the measured absorbance spectra. The absorption peak associated with carbon-poor phase is less pronounced than in the experiment due the neglect of excitonic effects [49], which enhances the absorption peak observed at about 200 nm in *h*-BN in particular due to the formation of exciton bound states with energies of 5.822 eV [50].

IV. SUMMARY

In summary, *ab initio* calculations have been combined with a rigorous statistical approach based on cluster expansion to study the effects of disorder, phase segregation, and composition fluctuations on $(BN)_{1-x}(C_2)_x$ monolayer alloy properties. We verified that the lattice parameters of the alloy follow Vegard's law and that there is no appreciable layer buckling. The strong tendency for phase separation that has been observed experimentally for intermediate compositions has been confirmed constructing the temperature-composition phase diagram. Electronic properties have been calculated using a state-of-the-art hybrid functional on the most statistically relevant cluster configurations. Concerning the electronic properties, we evaluate the energy gap and find that our results are in very good agreement with the experimental findings for the composition range in which the alloys are stable. The seemingly contradicting experimental findings for graphene above its solubility are explained in light of the phase separation process. We developed a methodology to obtain the optical absorbance spectra considering the phase-separated alloys within the GQCA statistical approach. The absorption results in a double peak, disregarding excitonic effects, showing very good agreement with experimental findings.

ACKNOWLEDGMENTS

We thank the Brazilian funding agencies FAPESP (Grant No. 2012/50738-3), CAPES (PVE Grant No. 88887.116535/2016-00), and CNPQ (Grant No. 311060/2013-7) for financial support. We also thank J. Furthmüller and P. B. Arruda for fruitful discussions and valuable support.

[1] Y. Chen, J. Xi, D. O. Dumcenco, Z. Liu, K. Suenaga, D. Wang, Z. Shuai, Y.-S. Huang, and L. Xie, ACS Nano **7**, 4610 (2013).
[2] M. Zhang, J. Wu, Y. Zhu, D. O. Dumcenco, J. Hong, N. Mao, S. Deng, Y. Chen, Y. Yang, C. Jin, S. H. Chaki, Y.-S. Huang, J. Zhang, and L. Xie, ACS Nano **8**, 7130 (2014).
[3] H. Li, X. Duan, X. Wu, X. Zhuang, H. Zhou, Q. Zhang, X. Zhu, W. Hu, P. Ren, P. Guo, L. Ma, X. Fan, X. Wang, J. Xu, A. Pan, and X. Duan, J. Am. Chem. Soc. **136**, 3756 (2014).
[4] B. Li, L. Huang, M. Zhong, N. Huo, Y. Li, S. Yang, C. Fan, J. Yang, W. Hu, Z. Wei, and J. Li, ACS Nano **9**, 1257 (2015).
[5] L. Ci, Nat. Mater. **9**, 430 (2010).
[6] C.-K. Chang, S. Kataria, C.-C. Kuo, A. Ganguly, B.-Y. Wang, J.-Y. Hwang, K.-J. Huang, W.-H. Yang, S.-B. Wang, C.-H. Chuang, M. Chen, C.-I. Huang, W.-F. Pong, K.-J. Song, S.-J. Chang, J.-H. Guo, Y. Tai, M. Tsujimoto, S. Isoda, C.-W. Chen, L.-C. Chen, and K.-H. Chen, ACS Nano **7**, 1333 (2013).
[7] Y. Gong, G. Shi, Z. Zhang, W. Zhou, J. Jung, W. Gao, L. Ma, Y. Yang, S. Yang, G. You, R. Vajtai, Q. Xu, A. H. MacDonald, B. I. Yakobson, J. Lou, Z. Liu, and P. M. Ajayan, Nat. Commun. **5**, 3193 (2014).
[8] Z. Liu, Nat. Nanotechnol. **8**, 119 (2013).
[9] D. Pacilé, J. C. Meyer, Ç. Ö. Girit, and A. Zettl, Appl. Phys. Lett. **92**, 133107 (2008).
[10] K. Yuge, Phys. Rev. B **79**, 144109 (2009).
[11] M. Ni, Y. Wang, Q. Yang, W. Zhu, Q. Tang, and Z. Li, Mod. Phys. Lett. B **28**, 1450144 (2014).
[12] R. D'Souza and S. Mukherjee, Physica E (Amsterdam, Neth.) **69**, 138 (2015).
[13] M. Kan, J. Zhou, Q. Wang, Q. Sun, and P. Jena, Phys. Rev. B **84**, 205412 (2011).
[14] M. S. C. Mazzoni, R. W. Nunes, S. Azevedo, and H. Chacham, Phys. Rev. B **73**, 073108 (2006).
[15] S. Azevedo, Phys. Lett. A **351**, 109 (2006).
[16] I. Guilhon, L. K. Teles, M. Marques, R. R. Pela, and F. Bechstedt, Phys. Rev. B **92**, 075435 (2015).
[17] L. K. Teles, J. Furthmüller, L. M. R. Scolfaro, J. R. Leite, and F. Bechstedt, Phys. Rev. B **62**, 2475 (2000).
[18] F. L. Freitas, J. Furthmüller, F. Bechstedt, M. Marques, and L. K. Teles, Appl. Phys. Lett. **108**, 092101 (2016).
[19] A. B. Chen and A. Sher, *Semiconductor Alloys* (Plenum, New York, 1995).

[20] A. Sher, M. van Schilfgaarde, A.-B. Chen, and W. Chen, Phys. Rev. B **36**, 4279 (1987).
[21] S. Kullback and R. A. Leibler, Ann. Math. Stat. **22**, 79 (1951).
[22] M. R. Uddin, J. Li, J. Y. Lin, and H. X. Jiang, J. Appl. Phys. **117**, 215703 (2015).
[23] G. Kresse and J. Furthmüller, Comput. Mater. Sci. **6**, 15 (1996).
[24] G. Kresse and J. Hafner, Phys. Rev. B **47**, 558(R) (1993).
[25] J. P. Perdew, K. Burke, and M. Ernzerhof, Phys. Rev. Lett. **77**, 3865 (1996).
[26] J. P. Perdew, K. Burke, and M. Ernzerhof, Phys. Rev. Lett. **78**, 1396 (1997).
[27] P. E. Blöchl, Phys. Rev. B **50**, 17953 (1994).
[28] G. Kresse and D. Joubert, Phys. Rev. B **59**, 1758 (1999).
[29] H. J. Monkhorst and J. D. Pack, Phys. Rev. B **13**, 5188 (1976).
[30] L. G. Ferreira, M. Marques, and L. K. Teles, Phys. Rev. B **78**, 125116 (2008).
[31] J. Heyd, G. E. Scuseria, and M. Ernzerhof, J. Chem. Phys. **118**, 8207 (2003).
[32] J. Heyd, G. E. Scuseria, and M. Ernzerhof, J. Chem. Phys. **124**, 219906 (2006).
[33] B. Adolph, V. I. Gavrilenko, K. Tenelsen, F. Bechstedt, and R. Del Sole, Phys. Rev. B **53**, 9797 (1996).
[34] M. Gajdoš, K. Hummer, G. Kresse, J. Furthmüller, and F. Bechstedt, Phys. Rev. B **73**, 045112 (2006).
[35] L. Matthes, O. Pulci, and F. Bechstedt, New J. Phys. **16**, 105007 (2014).
[36] S. Bhowmick, J. Rusz, and O. Eriksson, Phys. Rev. B **87**, 155108 (2013).
[37] Z. H. Huang, V. H. Crespi, and J. R. Chelikowsky, Phys. Rev. B **88**, 235425 (2013).
[38] A. van de Walle and G. Ceder, Rev. Mod. Phys. **74**, 11 (2002).
[39] M. R. Uddin, S. Majety, J. Li, J. Y. Lin, and H. X. Jiang, J. Appl. Phys. **115**, 093509 (2014).
[40] K. Raidongia, A. Nag, K. Hembram, U. Waghmare, R. Datta, and C. Rao, Chem. Eur. J. **16**, 149 (2010).
[41] A. R. Denton and N. W. Ashcroft, Phys. Rev. A **43**, 3161 (1991).
[42] L. Vegard, Z. Phys. **5**, 17 (1921).
[43] M. O. Watanabe, S. Itoh, T. Sasaki, and K. Mizushima, Phys. Rev. Lett. **77**, 187 (1996).
[44] B.-Y. Wang, H. Wang, L.-Y. Chen, H.-C. Hsueh, X. Li, J. Guo, Y. Luo, J.-W. Chiou, W.-H. Wang, P.-H. Wang, K.-H. Chen, Y.-C. Chen, L.-C. Chen, C.-H. Chen, J. Wang, and W.-F. Pong, Carbon **107**, 857 (2016).
[45] K. F. Mak, M. Y. Sfeir, Y. Wu, C. H. Lui, J. A. Misewich, and T. F. Heinz, Phys. Rev. Lett. **101**, 196405 (2008).
[46] R. R. Nair, P. Blake, A. N. Grigorenko, K. S. Novoselov, T. J. Booth, T. Stauber, N. M. R. Peres, and A. K. Geim, Science **320**, 1308 (2008).
[47] L. Matthes, P. Gori, O. Pulci, and F. Bechstedt, Phys. Rev. B **87**, 035438 (2013).
[48] L. Yang, J. Deslippe, C.-H. Park, M. L. Cohen, and S. G. Louie, Phys. Rev. Lett. **103**, 186802 (2009).
[49] T. T. K. Watanabe and H. Kanda, Nat. Mater. **3**, 404 (2004).
[50] B. Arnaud, S. Lebègue, P. Rabiller, and M. Alouani, Phys. Rev. Lett. **96**, 026402 (2006).